

Article

Design and Optimization of Multifunctional Human Motion Rehabilitation Training Robot EEGO

Kun Liu ^{*}, Shuo Ji, Yong Liu, Chi Gao, Jun Fu, Lei Dai and Shizhong Zhang

School of Mechanical and Aerospace Engineering, Jilin University, Changchun 130022, China

* Correspondence: kunliu@jlu.edu.cn

Abstract: A multifunctional human motion rehabilitation training robot named EEGO (electric easy go) that could achieve four functions through structural transformation was designed. The four functions achieved by four working modes: the Supporting Posture Mode (SM), the Grasping Posture Mode (GM), the Riding Posture Mode (RM), and the Pet Mode (PM), which are suitable for patients in the middle and late stages of rehabilitation. The size of the equipment under different functions is determined by the height of different postures of the human. During the design process, the equipment was lightweight using size optimization methods, resulting in a 47.3% reduction in mass compared to the original design. Based on the Zero Moment Point (ZMP) stability principle, the stability mechanism of the robot was verified under the three different functions. According to the wanted function of the equipment, the control system of the equipment was designed. Finally, a prototype was prepared based on the analysis and design results for experimental verification, which can effectively assist patients in motion rehabilitation training such as gait, walking, and other movements.

Keywords: rehabilitation robot; size optimization; ZMP; control system



Citation: Liu, K.; Ji, S.; Liu, Y.; Gao, C.; Fu, J.; Dai, L.; Zhang, S. Design and Optimization of Multifunctional Human Motion Rehabilitation Training Robot EEGO. *Actuators* **2023**, *12*, 311. <https://doi.org/10.3390/act12080311>

Academic Editor: Steve Davis

Received: 11 July 2023

Revised: 26 July 2023

Accepted: 27 July 2023

Published: 28 July 2023



Copyright: © 2023 by the authors. Licensee MDPI, Basel, Switzerland. This article is an open access article distributed under the terms and conditions of the Creative Commons Attribution (CC BY) license (<https://creativecommons.org/licenses/by/4.0/>).

1. Introduction

Aging issues affect various areas of society around the world. With an increase in age, the muscle strength of human will decrease, leading to gait disorder [1]. In addition, gait disorders are also common in stroke patients and Parkinson's patients [2,3]. Patients who suffer from gait impairment after the stroke need gait rehabilitation training to restore motor ability [4–6]. Gait rehabilitation training is an effective method to improve motor function, but it takes a long time [7].

In traditional rehabilitation therapy, physical therapists usually depend on manual rehabilitation for patients [8]. However, limited by the insufficient number of therapists at present, many patients cannot receive scientific rehabilitation training. In addition, unskilled physiotherapists will lead to decline of rehabilitation effect [9]. Robot-assisted rehabilitation training is considered to be an effective alternative as robots can meet the need for highly effective, targeted, and sustained rehabilitation training [10]. Therefore, to assist patients with scientific and long-lasting rehabilitation training and reduce the work pressure of physiotherapists, the research and development of rehabilitation robots is very important.

In recent years, with the development of robot technology, more and more rehabilitation robots appear [11]. However, most current rehabilitation robots, such as end-effector systems or exoskeleton-based systems, are mainly aimed at those patients in the early stage of rehabilitation. DDgo Pro is an end-effector type rehabilitation robot that uses a five-link mechanism to follow normal walking trajectory with three working modes: Passive Mode, Active Assisted Mode, and Active mode for different needs of patients. However, the structure and control system of the robot are complex for household use [12]. Mech-Walker is a lower extremity gait rehabilitation robot with a single actuator, which is based on

an optimized eight-bar Jansen's mechanism to generate a natural ankle trajectory during walking. However, the mechanism is also complicated and bulky for families [13]. A five degree-of-freedom (DOF) hybrid end-traction lower limb rehabilitation robot was designed for double-posture training (sitting posture/lying posture), but more appropriate EMG signal processing methods should be developed for the robot to complete more precise actions [14]. Lokomat is an exoskeleton rehabilitation robot, which consists of a pair of robotic arms, a body weight-supported treadmill system and exoskeleton, and the robot can assist stroke patients in gait training and help them recover. However, it is expensive and huge, making it affordable only for large hospitals or rehabilitation centers and is not suitable for home purchase and use by patients in the later stages of rehabilitation [15]. At the same time, there are many exoskeleton lower limb rehabilitation robots, which are wearable to drive patients to achieve sitting, standing, walking, and even running movements. And exoskeleton robot has more DOFs to help patients complete more complex rehabilitation training motions, but some exoskeleton rehabilitation robots are not very mature in human-computer interaction, which possibly leads to passive motion or inefficient rehabilitation training [16–18]. There is also a passive upper limb exoskeleton robot based on muscle kinematics model, which consists of the arm module, shoulder module, and back module, achieving bionic movement of upper limbs of patients [19]. The above examples show that the rehabilitation robot has rich functions and broad practical scenarios. In the design process of complex mechanical equipment, including rehabilitation robots, topology optimization methods are often used to complete the design of equipment. For example, in order to improve the payload capacity of the continuum robots in their curved configuration and solve the stress concentration problem of high-torsional-stiffness joints, a multiaxis design of flexure joints is achieved by a 3-D-topology-optimization-based method [20]. A cable-driven soft robotic gripper with multi-input and multi-output is developed using a topology optimization method, which could perform adaptive grasping, even rotating or panning the target [21]. In this paper, a multifunctional rehabilitation robot is designed, which can assist patients in achieving gait movements, serve as a transportation vehicle to carry patients for activities, and even serve as a pet to accompany patients.

Moreover, after the design of rehabilitation robot is completed, it is necessary to improve the portability and economy of the equipment and reduce the mass of the equipment. Using finite element analysis software to reduce the quality of equipment is a commonly used method. For example, in order to achieve lightweight of the shell of a certain device inside a spacecraft, the topology optimization method was successfully used to reduce the mass of the spacecraft shell by 36.8%, greatly reducing the launch cost of the spacecraft [22]. Finite element analysis software is used to calculate static force and mode of the bus body skeleton under four typical working conditions, optimize the size of the bus structure and components, and successfully reduce the mass of the bus body by 10.57% [23]. Topology optimization and size optimization are used to lighten a certain type of aircraft truss structure. In the process of optimization, topology optimization is used to obtain a new material distribution, and size optimization is used to get a new section size, which greatly reduces the mass of equipment and improves the performance of the aircraft [24]. Therefore, it is necessary to use finite element analysis software to perform lightweight analysis on the structure of the EEGO designed in this paper.

In this paper, we developed a multifunctional training rehabilitation robot, which could be used for patients in the middle and later stage of gait rehabilitation. It included four different working modes through structural transformation. Compared with traditional rehabilitation equipment, the robot was multifunctional with simple structure, which was conducive to household procurement and use. In Section 2, the overall design of the rehabilitation robot was introduced in detail and illustrated with pictures. In Section 3, the designed structure was lightweight through finite element analysis. In Section 4, the stability of equipment was analyzed. Section 5 conducted motor selection and the control system design. Section 6 provided the manufacturing process. Section 7 was the conclusion.

2. Functional and Structural Design

A multifunctional human motion rehabilitation training robot that could achieve four functions through structural transformation was designed with four modes: SM, GM, RM, and PM. The four modes could be switched according to user's needs and instructions as shown in Figure 1. EEGO could not only provide corresponding walking speeds based on the patient's gait rehabilitation condition but also effectively provide weight support and protection in preventing secondary injuries such as falls.

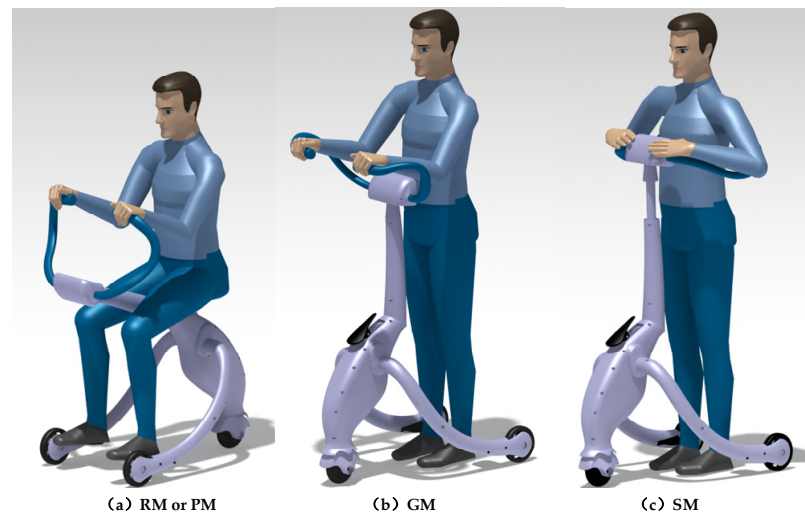


Figure 1. Different working modes of rehabilitation robot.

SM was designed for those patients in the middle stage of gait rehabilitation, who could only slowly stumble in a weight-supported state; the users can achieve weight support through underarm lifting mechanism according to his height and weight, thereby completing gait with lower upper body burden. GM was designed as walking aids for those patients in the late stage of gait rehabilitation whose walking ability has basically recovered, but need to grasp a handrail to gain a sense of psychological security during walking training. RM was applicable for fully recovered patients who need to ride short distances instead of walking indoors or outdoors to reduce physical exertion at a maximum speed of 12 km/h. PM was designed for entertainment needs of patients to eliminate loneliness. In this mode, EEGO could follow the user like a pet and switch the mechanical structures according to user's instructions at any time, achieving the entertainment function as an accompanying pet for solitary people. The difference between RM and PM was only the saddle posture. In PM, the saddle was regarded as a back wing of the companion pet and could be stirred up and down to indicate the pet's emotions, while in RM, the saddle was in a sitting position and provided seat for the user.

An adult male (weight 71 kg and height 1.75 m) was assumed to be the user of the motion rehabilitation training robot to conduct the structural design. According to the Human Dimensions of Chinese Adults [25], the size of the robot mechanical structure was calculated. Figure 2 showed different modes and the corresponding mechanical structure dimensions of the EEGO. The designed width (520 mm) was narrow enough to ensure that the robot possibly passed through various indoor entrances sufficiently. The designed height (1150 mm) in GM could meet the needs of most normal height users, and the height could be increased to 1400 mm from 1150 mm in SM to meet the height for underarm lifting of most users.

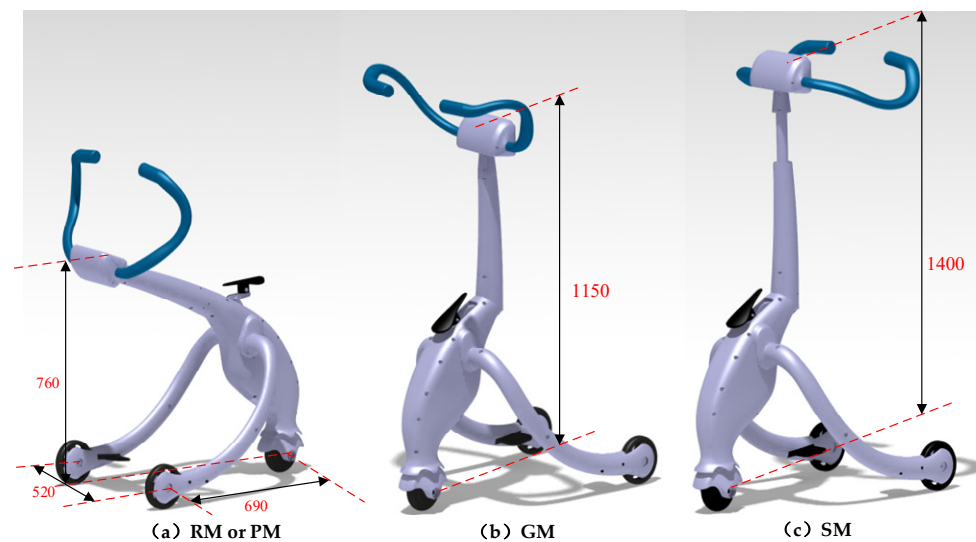


Figure 2. Size of different working modes of the designed rehabilitation robot.

EEGO included three main mechanisms: structural transformation mechanism, supporting mechanism, and chassis-driven mechanism, as shown in Figure 3. The structural transformation mechanism was located on top of and can rotate 180° around the supporting mechanism driven by an altitude-adjusting steering gear, achieving structural transformation between RM(PM) and SM(GM). As shown in Figure 3, brushless hub motor and a steering gear were installed on the chassis of EEGO, cooperating to drive the 301 driving and rudder wheel and 302 directional wheel to lead EEGO to anywhere the user wants to go. To achieve mechanical structure switched between different functional modes, two steering gears were employed to drive the two 101 handrails rotating around the horizontal axis of 102 head capsule to change the posture between GM and SM, and a push rod motor in the 103 Neck shell could lengthen or shorten to adjust the height of the structural transformation mechanism for users of different heights and weights.

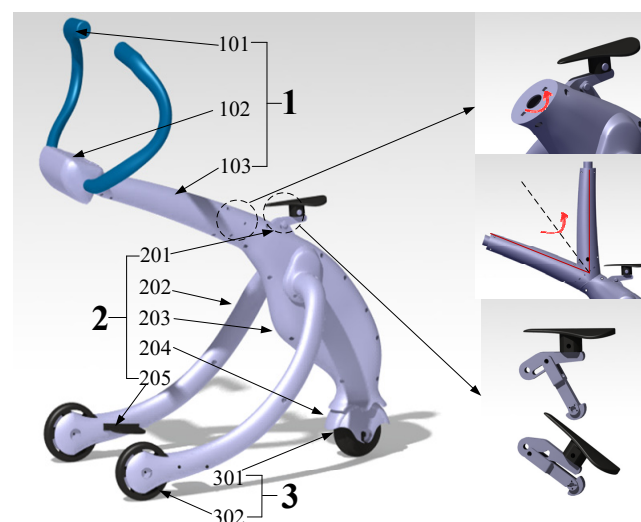


Figure 3. Mechanism design of EEGO. (1) Structural transformation mechanism: 101 handrail, 102 head capsule, and 103 neck shell. (2) Supporting mechanism: 201 saddle mechanism, 202 front rod, 203 main rod, 204 wheel fork, and 205 pedal. (3) Chassis-driven mechanism: 301 front wheel and 302 rear wheel.

3. Optimization of the Mechanism

EEGO was mainly designed for rehabilitation of patients, so while ensuring safety, the effective lightweight of the robot could improve portability and reduce manufacturing costs. The main load-bearing components of EEGO were thin-walled components, so that size optimization was used to design the mechanical structure for lightweight equipment [26]. The initial wall thickness of each member was 5 mm. The robot had four working modes, but the difference between PM and RM was only the posture of the saddle, and the bearing force of the equipment in RM with a rider was much greater than that in PM. Therefore, to improve analysis efficiency, only the mechanical structures in RM, GM, and SM were analyzed. The material was steel with density of 7850 kg/m^3 , Poisson's ratio of 0.3, elastic modulus of 210 GPa, and yield strength of 270 MPa.

3.1. Load Calculation in RM, GM, and SM

The load distribution of the mechanical structures in RM, GM, and SM was related to the quality of each limb segment of the user and the human–machine interaction status, which is shown in Figure 1. According to the inertia parameter table of Chinese adult human body, the weight of volunteers and the mass of each limb segment of human body could be obtained, as shown in Table 1 [27].

Table 1. Mass of each limb segment of human body.

Body Segments	Weight (kg)	Body Segments	Weight (kg)
Hand	0.454	Lower torso	19.3
Upper arm	1.72	Thigh	10.1
Forearm	0.887	Shank	2.61
Head and neck	6.12	Foot	1.05
Upper torso	11.9	-	-

In RM, the user sat on the saddle with feet on the pedals and hands on the handrails, as shown in Figure 1a. Based on the human–machine interaction state, the maximum pressure borne by the robot at each loaded position during RM was calculated, where the handrail bore the load from the hand grip and partial gravity of the hand, upper arm, and lower arm; the saddle bore the majority of the weight from the subject's whole body; the two pedals bore the load of stepping feet and partial gravity of the thighs, calves, and feet. The values of these loads are shown in Figure 4a. In GM or SM, the user stood within the range of two front rods with the hands grasping the handrails or with the armpit area pressing onto the transformed handrails, as shown in Figure 1b,c. Considering extreme working conditions, the user's weight was assumed to fully distributed to the handrail of the mechanism. Correspondingly, the force analysis of the mechanical structure is shown in Figure 4b,c.

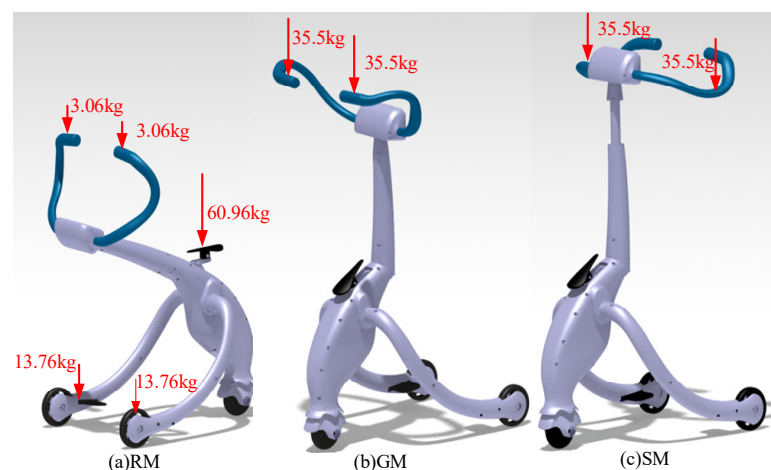


Figure 4. Force analysis of mechanisms in human–machine interactions in RM, GM, and SM.

3.2. Finite Element Analysis of the Mechanism

Three dimensional model was set up in CATIA software with fixed wheels and then imported to HyperWorks software for finite element analysis in gravity field with load according to the force analysis in Figure 4.

In the finite element analysis process, the load was uniformly applied to the corresponding load position (saddle, armrest, or pedal), and the three wheels of the chassis-driven mechanism are fixed. The preliminary resulted weight of the mechanism was 49.07 kg. The stress distribution of the mechanisms in RM, GM, and SM is shown in Figure 5. It could be seen that the maximum stress values of the three modes were all less than the allowable stress of steel, and the mechanism could be further lightweight.

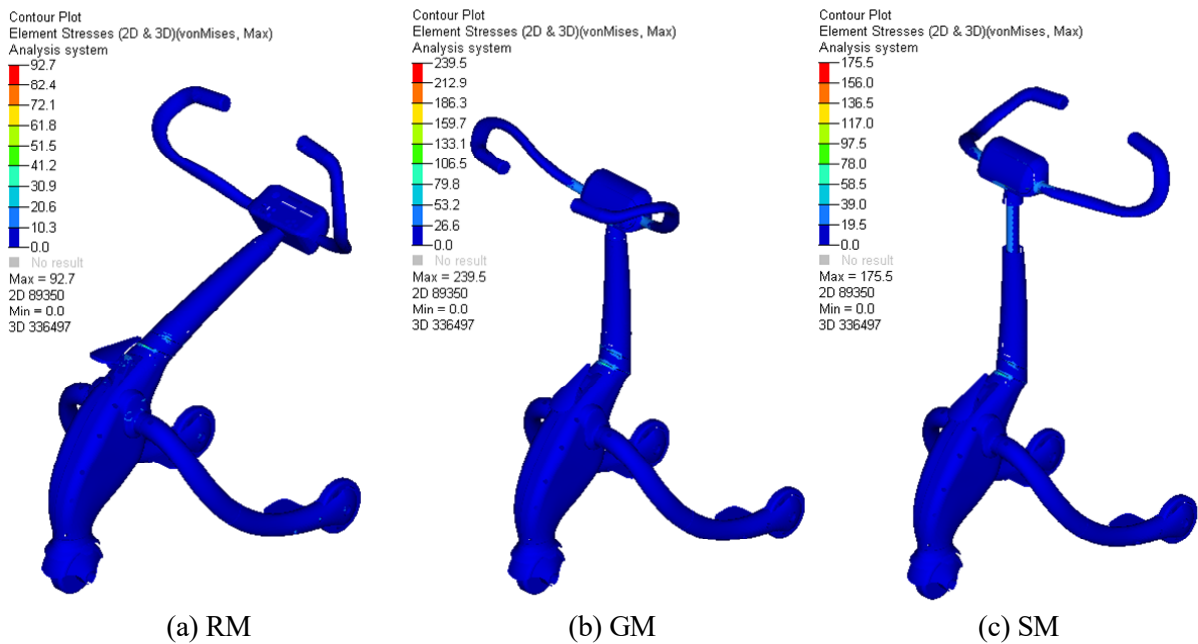


Figure 5. The stress distribution of the mechanisms in RM, GM, and SM.

Size optimization on the mechanisms in RM, GM, and SM was performed using Formula (1) where the thickness of all thin-walled components was the independent variable, the allowable stress of 270 MPa was the constraint condition, and the minimum mass was the objective function. And the optimization results are shown in Table 2.

$$\begin{cases} \min M = \sum_{i=1}^n m_i, i = 1, 2, \dots, n \\ m_i = f(x_i), i = 1, 2, \dots, n \\ \delta_{\max} \leq 270 \end{cases} \quad (1)$$

where the M is the mass of the mechanism; m_i ($i = 1, 2, 3, 4, 5, 6, 7, 8$) is the mass of handrail, head capsule, neck shell, main rod, front rod, wheel fork, pedal, and saddle mechanism, respectively; f is the mass function; x_i ($i = 1, 2, 3, 4, 5, 6, 7, 8$) is the wall thickness value of handrail, head capsule, neck shell, main rod, front rod, wheel fork, pedal, and saddle mechanism, respectively, where these wall thickness values of parts are design variables. δ_{\max} is the maximum stress.

The wall thickness values resulting from size optimization were reassigned to the components in RM, GM, and SM, and the corresponding stress values were obtained as shown in Figure 6. The results showed that all stress values were less than 270 Mpa, meeting the design requirements. The total mass of the mechanism had decreased from 49.07 kg to 25.87 kg with a decrease of 47.3%.

Table 2. Size optimization results in RM, GM, and SM.

Part	Original Thicknesses (mm)	Range of Thicknesses (mm)	Optimized Thicknesses in RM (mm)	Optimized Thicknesses in SM (mm)	Optimized Thicknesses in GM (mm)	Optimized Thicknesses (mm)	Final Integer Thicknesses (mm)
Handrail	5	1–10	1	1.53	1.32	1.53	2
Head capsule	5	1–10	1	3.969	3.33	3.969	4
Neck shell	5	1–10	1.53	3.89	3.37	3.89	4
Main rod	5	1–10	1	4.52	3.62	4.52	5
Front rod	5	1–10	1	1	1	1	1
Wheel fork	5	1–10	1	1	1	1	1
Pedal	5	1–10	1	1	1	1	1
Saddle mechanism	5	1–10	1.04	1	1	1.04	2

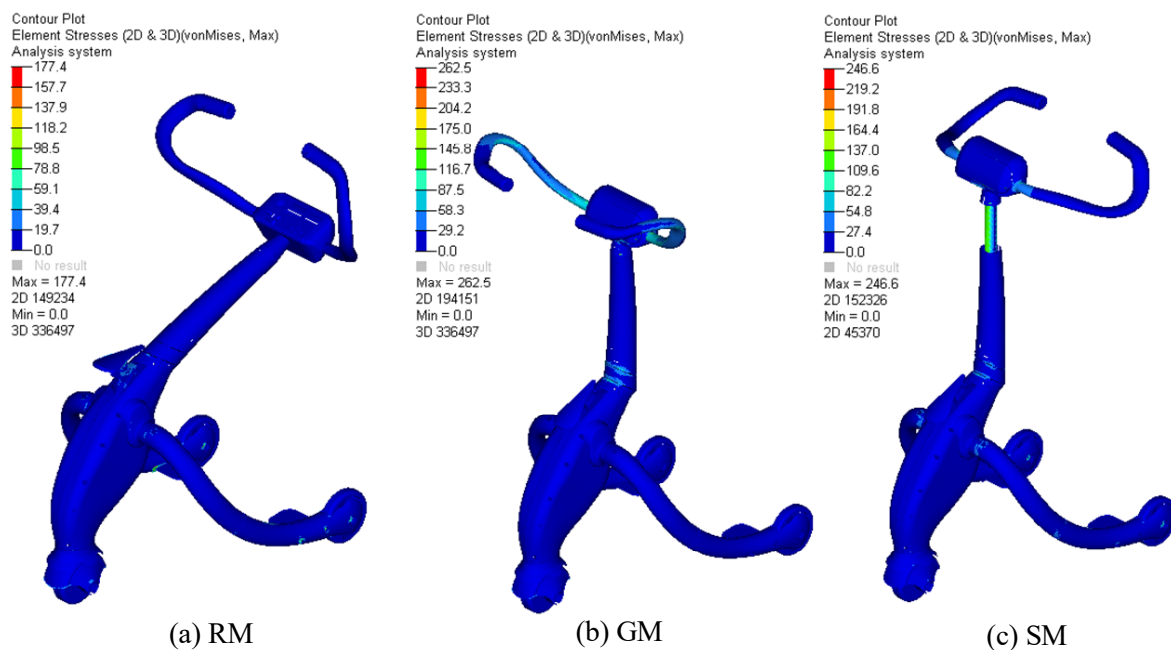


Figure 6. Stress value of components in RM, GM, and SM after size optimization.

4. Stability Analysis of the Mechanical System

The Zero Moment Point (ZMP) stability theory was often used as stability measurement of a mechanical system, which was related to the motion of the center of mass [28,29]. When the projection of ZMP was in the supporting polygon, the system was in the state of zero moment balance. In this part, the stability of the system was determined based on the projection position of the Zero Moment Point. Mechanism stability under human–machine interaction in RM, GM, and SM, as shown in Figure 7, was analyzed based on the ZMP stability theory. The ΔABC in Figure 7 was the stable area of the system. When the projection of ZMP was in ΔABC , the system was stable. PM could be considered as a special case of RM without rider. The ground projection points of human gravity, mechanism gravity, and the resultant force of them were all located inside ΔABC , and the action point of the resultant force of ground reaction should also be located inside ΔABC . Therefore, the projection of ZMP was in the supporting polygon, and the system was stable. The equipment could safely assist the patient to complete gait movements.

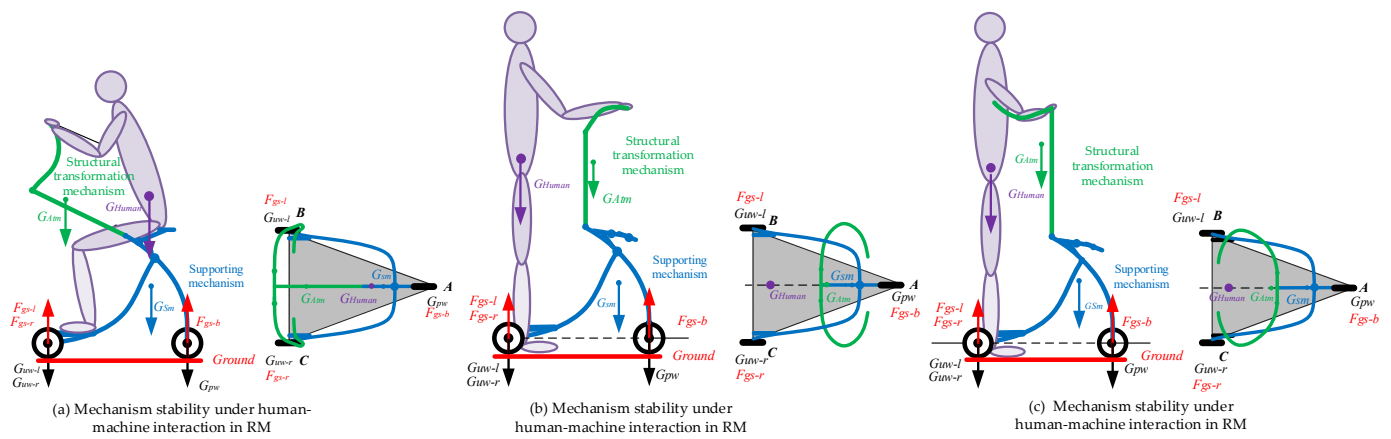


Figure 7. Analysis of mechanism stability under human machine interaction.

5. Motor Selection and Control System Design

Based on the optimized mass and size of the robot, as well as expected maximum weight of subjects to be carried, the power selection of the drive motors used in each function was carried out, and corresponding control systems were further designed based on the required operating functions under different working modes.

5.1. Motor Selection

As part of the electrical system design, it was necessary to calculate the motor driving torque of the robot during manned driving with maximum load as shown in Figure 8a, then select the motor. The output torque of the brushless hub motor was calculated as follows:

$$\begin{cases} T_1 \geq G_1 \cdot \sin \theta_1 \cdot h_1 + G_2 \cdot \sin \theta_1 \cdot h_2 - G_1 \cdot \cos \theta_1 \cdot \mu \cdot r - G_2 \cdot \cos \theta_1 \cdot \mu \cdot r \\ T_1 \leq G_1 \cdot \sin \theta_1 \cdot h_1 + G_2 \cdot \sin \theta_1 \cdot h_2 + G_1 \cdot \cos \theta_1 \cdot \mu \cdot r + G_2 \cdot \cos \theta_1 \cdot \mu \cdot r \end{cases} \quad (2)$$

where T_1 is the output torque of the brushless hub, G_1 and G_2 are the gravity of human seated on the saddle mechanism and the gravity of equipment, respectively, θ_1 is the maximum climbing angle of the equipment, r is the radius of rear wheel, h_1 is the vertical distance between the center of front wheel and the center of the rear wheel, h_2 is the vertical distance between the center of gravity of the equipment and the center of the rear wheel, and μ is the friction coefficient.

Altitude adjusting steering gear was the key component that drives the structural transformation mechanism to rotate around the supporting mechanism driven within 180-degree to achieve structural transformation between RM(PM) and SM(GM). The force analysis of the altitude adjusting steering gear is shown in Figure 8b, whose maximum torque was calculated as follows:

$$T_2 = G_3 \cdot \cos \theta_2 \cdot d_1 + G_4 \cdot \cos \theta_2 \cdot d_2, \quad (3)$$

where T_2 is the output torque of the altitude adjusting steering gear, G_3 and G_4 are the gravity of the head shell and the rotating neck, respectively, d_1 and d_2 are the force arms of the head shell and rotating neck to the rotating shaft of the altitude adjusting steering gear, respectively, and θ_2 is the included angle between the axis and the horizontal direction of the rotating neck after 90-degree clockwise rotation.

Specific parameters of all the power components in the electrical system are shown in Table 3. The hardware control schematic diagram and working logic flow chart of EEGO are shown in Figures 9 and 10.

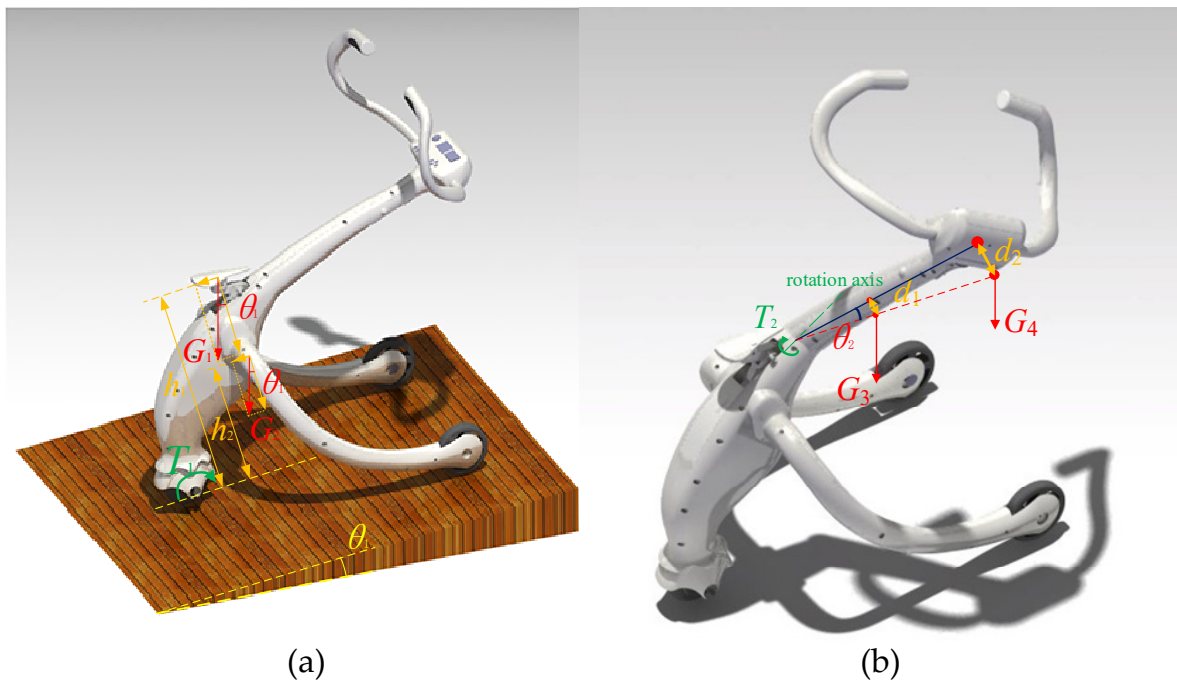


Figure 8. Force analysis of equipment: (a) Force analysis in RM; (b) Force analysis of altitude adjusting steering gear.

Table 3. Parameters of power components.

Power Components	Rated Voltage (V)	Rated Torque (N m)/Thrust (N)
hub motor	24	20 N m
steering gear	6	2.5 N m
seat altitude adjusting steering gear	6	2.5 N m
altitude adjusting steering gear	6	6 N m
handrail adjusting steering gear	6	2.5 N m
push-rod motor	24	100 N

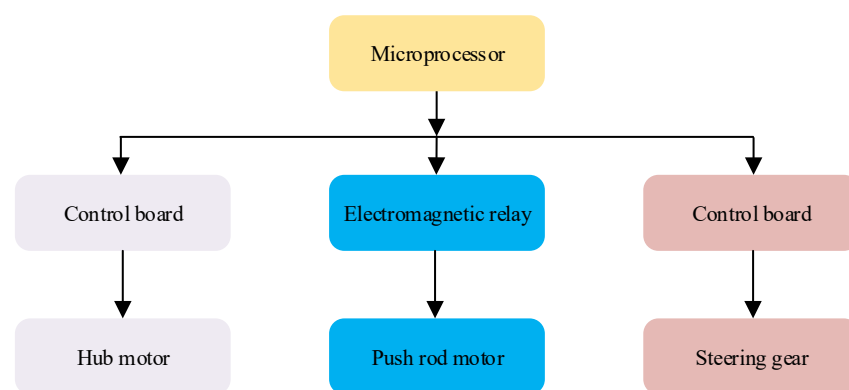


Figure 9. Hardware system control schematic diagram.

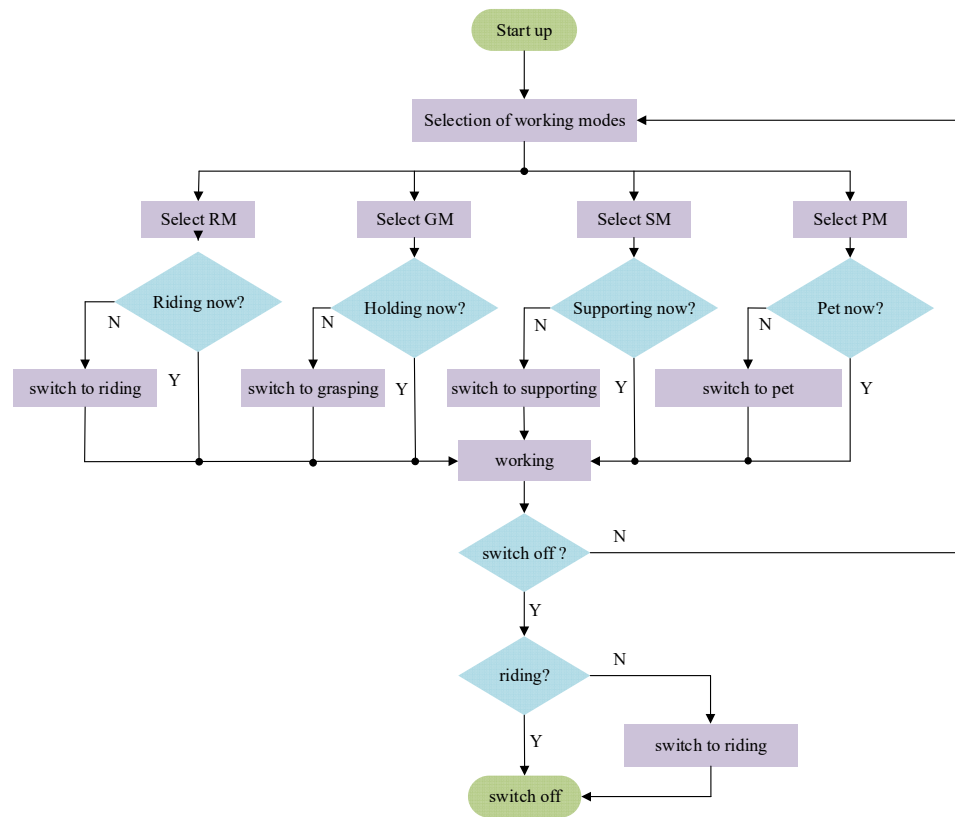


Figure 10. Work flow chart of EEGO.

5.2. Control System Design

5.2.1. Riding Posture Mode

In RM, EEGO was used as a vehicle, which could provide speeds in three gears for users: slow speed (3 km/h), medium speed (6 km/h), and fast speed (12 km/h). After selecting the initial speed gear, the current speed could also be adjusted with a variation of 1 km/h through acceleration or deceleration commands during driving. In the speed control, a PWM wave with different duty cycles was used as the control signal to adjust the speed. It was necessary to analyze the relationship between the steering angle and the maximum turning speed to prevent EEGO from tipping over due to excessive turning speed during turning. When EEGO detects that the turning speed was close to the maximum allowable turning speed under the current steering angle, it would automatically slow down to prevent tipping and thus avoid user injury. The relationship between the steering angle of the driving wheel of the equipment and the maximum turning speed was as follows:

$$v_{\max}^2 = \frac{l \cdot g \cdot \mu}{k \cdot \sin \theta'} \tag{4}$$

where v_{\max} is the maximum turning speed of EEGO, l is the track width of the front and rear wheels, g is the acceleration of gravity, μ is the coefficient of friction, k is the safety factor, which was taken as 1.5 here, and θ is the steering angle of the driving wheel.

The correlation diagram between the steering angle of the driving wheel and the maximum turning speed is shown in Figure 11.

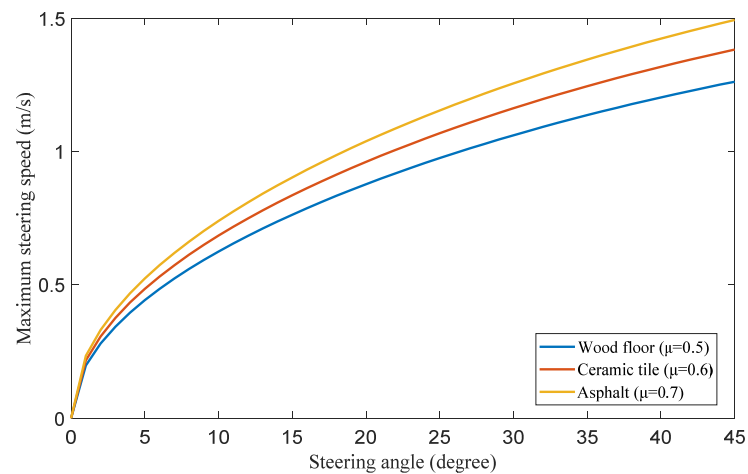


Figure 11. The correlation diagram between the steering angle of the driving wheel and the maximum turning speed.

5.2.2. Grasping Posture Mode

In GM, when the user grasps the corresponding position of the handrails, the heart rate sensor at that position begins to work. When the user's heart rate was monitored to reach 110 bpm, it would automatically brake and issue a warning to remind the user of abnormal physical condition. The hub motor was in constant speed control mode to prevent the device from sliding up and down a slope resulting in injury to the user. When the torque that the hub motor could provide was not enough to maintain the current speed, the hub motor would automatically stop and self-lock to prevent slipping.

5.2.3. Supporting Posture Mode

In SM, the two handrails were raised and rotated to a horizontal position for the user's upper limbs to be placed flat on, providing support and assistance for the user. The hub motor was also in constant speed control mode at three alternative speeds (1 km/h, 2 km/h, or 3 km/h) to meet those of patients in the middle stage of gait rehabilitation, who can only slowly stumble in a weight-supported state. When the user feels tired during gait rehabilitation training, he could control the EEGO shutdown at any time through the control panel.

5.2.4. Pet Mode (PM)

In PM, the user could control the hub motor and steering motor of EEGO through a remote control to change its speed and direction, thereby simulating the ground motion state of a pet at different speeds and turning postures.

At the same time, the saddle mechanism could also be driven by an embedded drive motor to achieve posture adjustment of fixed axis lifting or lowering, simulating state of flapping wings as an insect does to provide users with fun companionship.

6. Manufacture and Evaluation of Prototype

Based on the above functional design and structural optimization, a prototype was manufactured, which contains multiple components, including control boards, microprocessors, batteries, transformers, and various drive motors. To reduce the volume of the prototype body and head, it was necessary to coordinate the installation positions of various components inside the body and head. The installation and distribution positions of the parts are shown in Figure 12. The electric circuit flow chart of the equipment is shown in Figure 13.

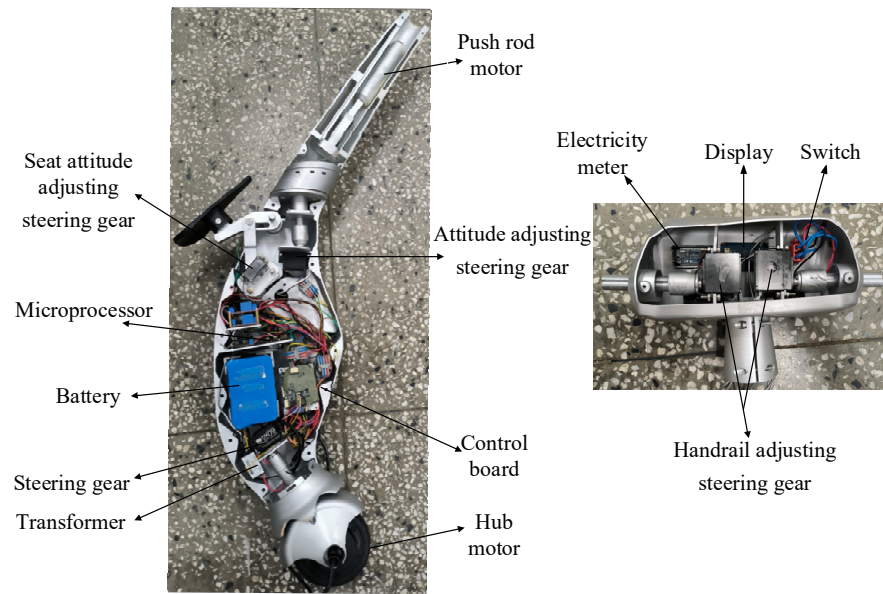


Figure 12. Installation and distribution positions of the parts.

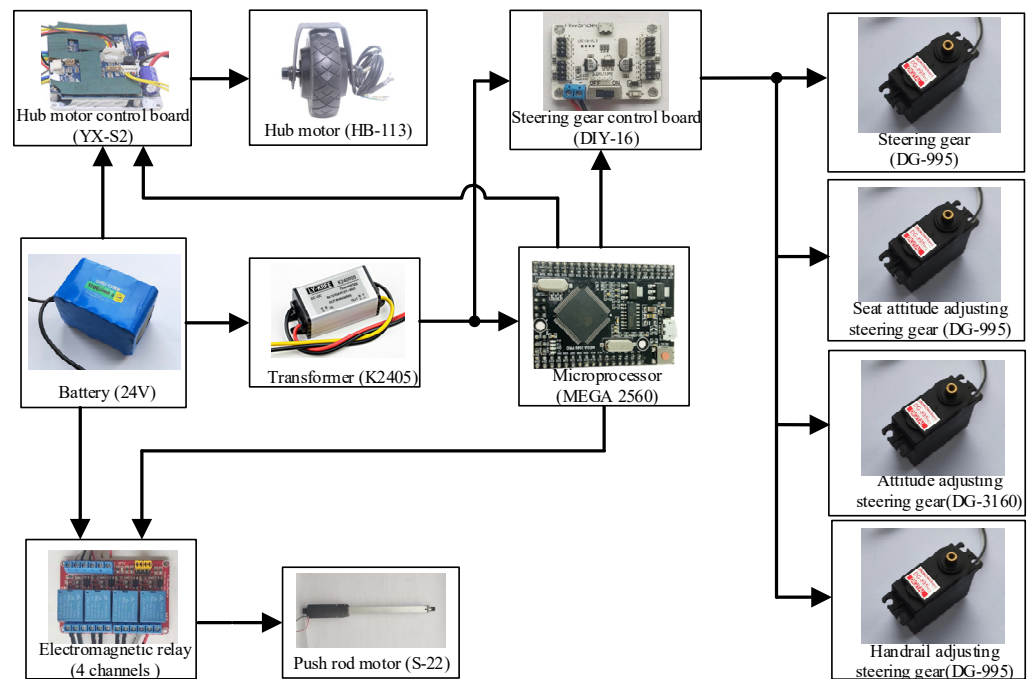


Figure 13. The electric circuit flow chart of the equipment.

The structural transformation mechanism was located on top of and can rotate 180-degree counterclockwise around the supporting mechanism from inclined state to vertical state, driven by an altitude adjusting steering gear, and achieved structural transformation between RM(PM) and SM(GM). The seat altitude adjusting steering gear can rotate 25-degree clockwise, so that the user can alight from the saddle. In the process of the equipment changing from the GM to SM, the handrail adjusting steering gear could rotate 180-degree clockwise to drive the handrail to rotate, and then the push-rod motor could be raised to the corresponding position. The conversion process between different modes is shown in Figure 14.

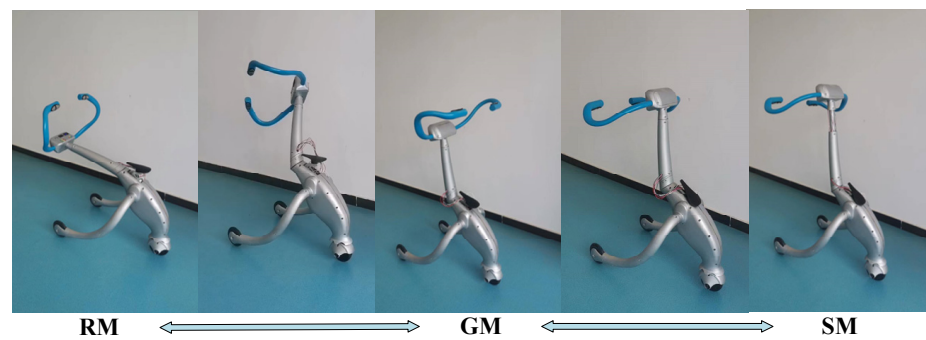


Figure 14. Function switching between each mode.

In this part, the functionality of the EEGO was evaluated through experiments. The main function was to assist the patient's gait, reduce the pressure on the lower limbs during the gait, and sometimes it could also be used as a mobile equipment to help the patient movement. The RM and PM were basic functions without structure transformation that were not needed to verify. In order to verify the function of EEGO in GM and SM, six volunteers (age = 25 ± 3 years, mass = 70 ± 10 kg, height = 170 ± 10 cm) participated in experiments. All the six volunteers had no lower limb diseases and could complete gait movement independently. During the experiment, volunteers first performed gait movement without EEGO's assistance, then performed gait movement with EEGO's assistance in GM and PM, respectively, and filled out the usage perception questionnaire. The experimental protocol was approved by the Human Ethical Review Committee of the First Hospital of Jilin University (No. 2023-258). Written and verbal instructions of testing procedures were provided, and written consent was obtained from the subject prior to testing. The distance of each gait movement was 20 m. In order to avoid the interference between consecutive gait movements, the volunteers should rest fully after each gait movement before proceeding to the next one. The operation process of a volunteer performing experiments in both GM and PM is shown in Figure 15. The results of the usage perception questionnaire are shown in Table 4.

The results showed that the power-assisted effect of the equipment was good, and the design goal of the equipment was achieved.

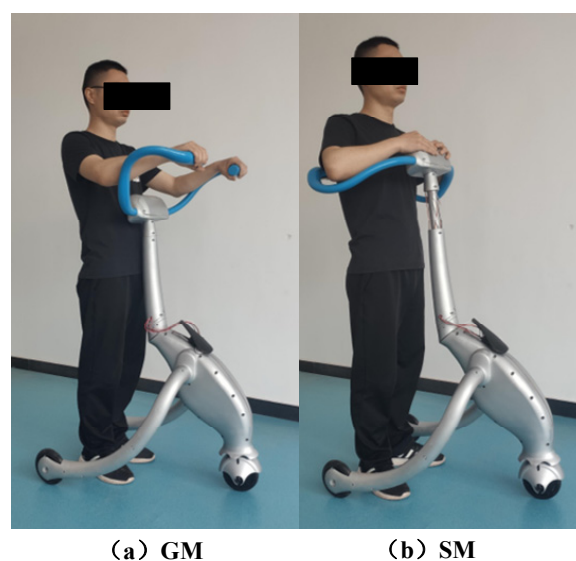


Figure 15. The operation process of a volunteer performing experiments in both GM and PM.

Table 4. The results of the questionnaire of six volunteers.

Volunteers	Feeling in GM	Feeling in SM
Volunteer 1	Relaxing	Relaxing
Volunteer 2	Relaxing	Relaxing
Volunteer 3	Relaxing	Relaxing
Volunteer 4	Relaxing	Relaxing
Volunteer 5	Relaxing	Relaxing
Volunteer 6	Relaxing	Relaxing

7. Conclusions

Rehabilitation equipment was very important for promoting patients' rehabilitation and reducing the work pressure of medical staff. A multifunctional human motion rehabilitation training robot named EEGO that could achieve four functions (RM, SM, GM, AM) through structural transformation was designed and optimized. EEGO were suitable for patients in the middle and late stages of rehabilitation. The weight of the equipment was light, and the size of the equipment was suitable for indoor use. Finally, a prototype was prepared based on the analysis and design results of experimental verification, which could effectively assist patients in motion rehabilitation training such as gait, walking, and other movements.

In future research work, we would further reduce the weight of the equipment by changing the types of materials. In addition, we would further optimize the internal space of the equipment, reasonably placing the motor, battery, and other parts to reduce the size and weight of the equipment.

Author Contributions: K.L.: Writing—review and editing, methodology, and conceptualization. S.J.: Writing—original draft, software, methodology, formal analysis, and data curation. Y.L.: Visualization, validation, methodology, and investigation. C.G.: Investigation and supervision. J.F.: Project administration and formal analysis. L.D.: Software and methodology. S.Z.: Data curation. All authors have read and agreed to the published version of the manuscript.

Funding: This research received no external funding.

Institutional Review Board Statement: Not applicable.

Informed Consent Statement: Not applicable.

Data Availability Statement: Data are unavailable due to privacy or ethical restrictions.

Acknowledgments: The authors wish to acknowledge the support of the volunteer subjects of Robotics and Dynamics Research Lab at Jilin University.

Conflicts of Interest: The authors declare no conflict of interest.

References

- Lizeth, H.S.; Susanne, M.; Steven, T.; Wim, S.; Katja, M.; Ann, H.; Tamay, V.C. Decline in gait propulsion in older adults over age decades. *Gait Posture* **2021**, *90*, 475–482.
- Li, D.; Zha, F.; Long, J.; Liu, F.; Gao, J.; Wang, Y. Effect of Robot Assisted Gait Training on Motor and Walking Function in Patients with Subacute Stroke: A Random Controlled Study. *J. Stroke Cerebrovasc. Dis.* **2021**, *30*, 105807. [[CrossRef](#)] [[PubMed](#)]
- Cecilia, R.; Jorik, N.; Bastiaan, R.B.; Marina, P.; Christian, B.; Klaus, S.; Gregor, K.W. Gait and Postural Disorders in Parkinsonism: A Clinical Approach. *J. Neurol.* **2020**, *267*, 3169–3176.
- Vaida, C.; Carbone, G.; Major, K.; Major, Z.; Plitea, N.; Pisla, D. On human robot interaction modalities in the upper limb rehabilitation after stroke. *Acta Tech. Napoc. Ser. -Appl. Math. Mech. Eng.* **2017**, *60*, 91–102.
- Tucan, P.; Vaida, C.; Plitea, N.; Pisla, A.; Carbone, G.; Pisla, D. Risk-based assessment engineering of a Parallel Robot used in post-stroke upper limb rehabilitation. *Sustainability* **2019**, *11*, 2893. [[CrossRef](#)]
- Benson, I.; Hart, K.; Tussler, D.; Van Middendorp, J.J. Lower-limb exoskeletons for individuals with chronic spinal cord injury: Findings from a feasibility study. *Clin. Rehabil.* **2016**, *30*, 73–84. [[CrossRef](#)]
- Bishnoi, A.; Lee, R.; Hu, Y.; Mahoney, J.R.; Hernandez, M.E. Effect of Treadmill Training Interventions on Spatiotemporal Gait Parameters in Older Adults with Neurological Disorders: Systematic Review and Meta-Analysis of Randomized Controlled Trials. *Int. J. Environ. Res. Public Health* **2022**, *19*, 2824. [[CrossRef](#)]

8. Zhang, J.F.; Dong, Y.M.; Yang, C.J.; Geng, Y.; Chen, Y.; Yang, Y. 5-Link model based gait trajectory adaption control strategies of the gait rehabilitation exoskeleton for post-stroke patients. *Mechatronics* **2010**, *30*, 368–376. [[CrossRef](#)]
9. Feng, J.; Laurence, T.Y.; Zhang, R.; Qiang, W.; Chen, J. Privacy Preserving High-Order Bi-Lanczos in Cloud-Fog Computing for Industrial Applications. *IEEE Trans. Ind. Inform.* **2022**, *18*, 7009–7019. [[CrossRef](#)]
10. Lo, K.; Stephenson, M.; Lockwood, C. Effectiveness of robotic assisted rehabilitation for mobility and functional ability in adult stroke patients: A systematic review protocol. *JBI Database Syst. Rev. Implement. Rep.* **2017**, *15*, 39–48. [[CrossRef](#)]
11. Zhou, J.; Yang, S.; Xue, Q. Lower limb rehabilitation exoskeleton robot: A review. *Adv. Mech. Eng.* **2021**, *13*, 1–17. [[CrossRef](#)]
12. Kim, J.Y.; Kim, J.Y.; Kim, H.C.; Park, K. Development and Evaluation of a Hybrid Walking Rehabilitation Robot, DDgo Pro. *Int. J. Precis. Eng. Manuf.* **2020**, *21*, 2015–2115. [[CrossRef](#)]
13. Haghjoo, M.R.; Lee, H.; Afzal, M.R.; Eizad, A.; Yoon, J. Mech-Walker: A Novel Single-DOF Linkage Device With Movable Frame for Gait Rehabilitation. *IEEE/ASME Trans. Mechatron.* **2021**, *26*, 13–23. [[CrossRef](#)]
14. Wang, L.P.; Tian, J.J.; Du, J.Z. A Hybrid Mechanism-Based Robot for End-Traction Lower Limb Rehabilitation: Design, Analysis and Experimental Evaluation. *Machines* **2022**, *10*, 99. [[CrossRef](#)]
15. Alashram, A.R.; Annino, G.; Padua, E. Robot-assisted gait training in individuals with spinal cord injury: A systematic re-view for the clinical effectiveness of Lokomat. *J. Clin. Neurosci.* **2021**, *91*, 260–269. [[CrossRef](#)] [[PubMed](#)]
16. Hybart, R.L.; Ferris, D.P. Embodiment for Robotic Lower-Limb Exoskeletons: A Narrative Review. *IEEE Trans. Neural Syst. Rehabil. Eng.* **2023**, *31*, 657–688. [[CrossRef](#)] [[PubMed](#)]
17. Campbell, S.M.; DIduch, C.P.; Sensinger, J.W. Autonomous Assistance-as-needed control of a lower limb exoskeleton with guaranteed stability. *IEEE Access* **2020**, *8*, 51168–51178. [[CrossRef](#)]
18. Yu, H.; Huang, S.; Chen, G.; Pan, Y.; Guo, Z. Human robot interaction control of rehabilitation robots with series elastic actuators. *IEEE Trans. Robot.* **2015**, *31*, 1089–1100. [[CrossRef](#)]
19. Ning, Y.; Li, Y.; Zhang, Z.; Liu, K.; Liu, J.; Cai, J.; Wang, C. Structure design and analysis of upper limb wearable passive power-assisted exoskeleton robot. *J. Phys. Conf. Ser.* **2023**, *2489*, 012008. [[CrossRef](#)]
20. Sun, Y.; Lueth, T.C. Enhancing Torsional Stiffness of Continuum Robots Using 3-D Topology Optimized Flexure Joints. *IEEE/ASME Trans. Mechatron.* **2023**, 1–9. [[CrossRef](#)]
21. Wang, R.; Zhang, X.; Zhu, B.; Zhang, H.; Chen, B.; Wang, H. Topology optimization of a cable-driven soft robotic gripper. *Struct. Multidiscip. Optim.* **2022**, *62*, 2749–2763. [[CrossRef](#)]
22. Yu, G.; Feng, J.; Pan, G.; Yan, G. Lightweight Design of Shell Based on Finite Element Method. *J. Phys. Conf. Ser.* **2023**, *2501*, 012014.
23. Yao, C.; Yang, M. Research on Lightweight Design and Finite Element Analysis of a 9 Meter Bus Body Frame. *J. Phys. Conf. Ser.* **2021**, *1748*, 062022. [[CrossRef](#)]
24. Qiu, J.; Fan, Y.; Wei, H.; Zhang, P. Lightweight design of aircraft truss based on topology and size optimization. *J. Phys. Conf. Ser.* **2021**, *1986*, 012094. [[CrossRef](#)]
25. GB/T 10000-1988; Standardization Administration of the People’s Republic of China. Human Dimensions of Chinese Adults. Standardization Administration of the People’s Republic of China: Beijing, China, 1988.
26. Pan, Y.; Xiong, Y.; Wu, L.; Diao, K.; Guo, W. Lightweight Design of an Automotive Battery-Pack Enclosure via Advanced High-Strength Steels and Size Optimization. *Int. J. Automot. Technol.* **2021**, *22*, 1279–1290. [[CrossRef](#)]
27. GB/T 17245-2004; Standardization Administration of the People’s Republic of China. Inertial Parameters of Adult Human Body. Standardization Administration of the People’s Republic of China: Beijing, China, 2004.
28. Zheng, Y.; Wang, Y.; Liu, J. Analysis and experimental research on stability characteristics of squatting posture of wearable lower limb exoskeleton robot. *Future Gener. Comput. Syst.* **2021**, *125*, 352–363. [[CrossRef](#)]
29. Kim, S.H.; Hong, Y.D. Dynamic Bipedal Walking Using Real-Time Optimization of Center of Mass Motion and Capture Point-Based Stability Controller. *J. Intell. Robot. Syst.* **2021**, *103*, 58. [[CrossRef](#)]

Disclaimer/Publisher’s Note: The statements, opinions and data contained in all publications are solely those of the individual author(s) and contributor(s) and not of MDPI and/or the editor(s). MDPI and/or the editor(s) disclaim responsibility for any injury to people or property resulting from any ideas, methods, instructions or products referred to in the content.